

# Density functional study of atomic and electronic structures of graphene on the FePd(001) surface

Mitsuharu Uemoto,<sup>1, a)</sup> Hayato Adachi,<sup>1</sup> Hiroshi Naganuma,<sup>2, 3, 4, 5</sup> and Tomoya Ono<sup>1</sup>

<sup>1)</sup>Department of Electrical and Electronic Engineering, Graduate School of Engineering, Kobe University, 1-1 Rokkodai-cho, Nada-ku, Kobe 651-8501, Japan

<sup>2)</sup>Center for Innovative Integrated Electronics Systems (CIES), Tohoku University, 468-1 Aramaki Aza Aoba, Aoba, Sendai, Miyagi, 980-8572, Japan

<sup>3)</sup>Center for Spintronics Integrated Systems (CSIS), Tohoku University, 2-2-1 Katahira Aoba, Sendai, Miyagi 980-8577 Japan

<sup>4)</sup>Center for Spintronics Research Network (CSRN), Tohoku University, 2-1-1 Katahira, Aoba, Sendai, Miyagi 980-8577 Japan

<sup>5)</sup>Graduate School of Engineering, Tohoku University, 2-1-1 Katahira, Aoba, Sendai, Miyagi 980-8579, Japan

(Dated: 24 November 2023)

We report on the investigation of the atomic-scale structure and electronic properties of graphene(Gr) on the  $L1_0$ -FePd(001) interface using density functional theory. Although such hetero-interfaces have been experimentally synthesized, due to the significant lattice symmetry mismatch between the graphene and tetragonal alloy surface, a theoretical understanding of the optimal configuration of the carbon atoms is required. In this work, we consider various model structures of twisted and non-twisted FePd(001)/Gr interfaces. To evaluate the stability of our models, we analyzed the adsorption energies per carbon atom by performing structural optimizations, including van der Waals interactions. We found that the most stable structure had an adsorption energy of approximately  $\approx -0.109$  eV/atom ( $-10.5$  kJ/mol), and the energy barrier of the slide was smaller than  $0.05$  meV/atom. The FePd-graphene distance was approximately  $2$  Å, which successfully reproduced the experimental value.

Keywords: Spintronics, First-principles, FePd

## I. INTRODUCTION

Iron-palladium<sup>1–11</sup> is a binary ordered alloy with tetragonal  $L1_0$  structure that has attracted much attention as a material for spintronic applications<sup>1,2</sup> due to its high perpendicular magnetic anisotropy (PMA) of  $K_u \sim 10^7$  erg/cm<sup>33–5</sup>, and low Gilbert damping of thin films ( $\alpha \sim 10^{-2}$ )<sup>8,9</sup>. These properties are desirable for high-density magnetic random access memory (MRAM)<sup>12</sup> and magnetic tunneling junction (MTJ)<sup>2</sup> devices. However, when FePd forms an interface with the MgO tunnel barrier, the lattice mismatch approaches 10 %, which is a serious problem for a smooth interface and obtaining a high tunnel magnetoresistance (TMR) ratio.

In a recent experiment, the integration of graphene layers deposited on the (001)-surface of FePd (FePd(001)/Gr) was successfully realized using chemical vapor deposition (CVD)<sup>6</sup>. It has been reported that graphene protects Fe atoms on the surface from oxidation and provides stable crystallinity, atomic thickness, and flatness controls without degrading the perpendicular magnetic properties. Graphene grown by CVD is expected to have an energetically stable orientation when formed on tetragonal FePd epitaxial films. In contrast to the MgO barrier and FePd interface, van

der Waals force bonding can be expected to form a flat interface between the graphene and FePd layers. However, the actual atomic configuration of C atoms on the surface is not yet well understood.

In general, the graphene on metal surfaces has been studied experimentally and theoretically, especially for fcc metal (*e.g.*, Ni(111)/Gr, Cu(111)/Gr, Al(111)/Gr, etc.)<sup>13–18</sup>. The (111)-surface of fcc crystals has a three-fold symmetry, which is in good agreement with the honeycomb structure of graphene; the C atoms are placed on characteristic "adsorption sites" relative to surface metallic atoms<sup>13</sup>. In addition, the bonding mechanism of the metal-graphene interfaces can be divided into two regimes: physisorption and chemisorption<sup>14</sup>. In the former case, graphene is weakly attracted to the metallic atoms by van der Waals (vdW) interactions. In the latter case, a strong hybridization between the graphene  $p\pi$ -state and metal  $d$ -state modifies the electronic band structure and shortens the graphene-metal distances; *for example*, the typical physisorbed and chemisorbed distances are estimated as  $\sim 3$  Å and  $\sim 2$  Å, respectively<sup>14</sup>. On the other hand, for the tetragonal  $L1_0$  structure and graphene, such as FePd(001)/Gr, Fe (or Pd) atoms on the (001) face are arranged in a square lattice that is mismatched with the graphene honeycomb. Therefore, the atomic configuration on the interface and the bonding mechanism are not as obvious as those with the fcc-metal surfaces.

In this work, we propose a simple model describing the atomic-scale interface structure of FePd(001)/Gr. Our

<sup>a)</sup>Electronic mail: uemoto@eedept.koe-u.ac.jp.

models are designed by guidelines considering the attractive interaction between C and Fe atoms and the strain on the honeycomb structure of graphene. We consider a few different supercell structures and analyze the difference in their binding energies using first-principles calculations. To find out the conditions for a stable structure, we analyze the influence of the bond length and angle of the C atoms and the relative displacement to the top-most Fe atoms. We also investigate twisted surfaces with a few different angles. According to the electronic state analysis, the magnetic properties of FePd are not affected by the presence of graphene, which is in good agreement with recent experiments<sup>1</sup>. To understand the adsorption mechanism, the distribution of C-Fe distances was investigated, and the interlayer distance in our calculation agreed well with the value determined by electron microscopy.

The remainder of this paper is organized as follows. II, we present the interface structures considered in this study and the computational conditions. In Sec. III, we report the optimized energies of each structure and discuss their electronic structures. Finally, in Sec. IV, we conclude our study.

## II. METHOD

Figure 1(a) shows the bulk FePd unit cell, which contains single Fe and Pd atoms; The lattice parameters are  $a_{\text{FePd}} = 2.67 \text{ \AA}$ , and  $c_{\text{FePd}} = 3.70 \text{ \AA}$ , which are determined from the structural optimization under equilibrium conditions, in good agreement with previous experimental and theoretical studies<sup>7,10,11</sup>. Figure 1(b) illustrates the honeycomb lattice structure of the graphene; the gray rectangle area is a single unit cell, containing four carbon atoms in each cell; the in-plane inter-atomic distance is  $a_{\text{Gr}} = 1.42 \text{ \AA}$ . Owing to the difference in lattice symmetry between FePd and graphene, the atomic interface structures are not obvious.

In this work, we propose a simple structural model of the FePd(001)/Gr interface; as seen Fig. 1(c), the arm-chair (AC) and zigzag (ZZ) directions of the graphene layer are parallel to the [100] and [010] directions of FePd, respectively. This structure is found from the following guiding principles: 1. Due to the attractive interaction between Fe and C atoms, the arrangement in which these atoms are considered to be stable. 2. The honeycomb structure of graphene on the surface should not have significant distortions. The period of the graphene ZZ direction  $\sqrt{3}a_{\text{Gr}} = 2.46 \text{ \AA}$  is relatively close to that of  $a_{\text{FePd}}$ ; the strain in this direction is expected to be small. However, because the period of the AC direction  $3a_{\text{Gr}} = 4.26 \text{ \AA}$  has a significant mismatch with  $a_{\text{FePd}}$ , a long-period supercell structure is required in this direction. We refer to the interface structure consisting of  $n$ -period FePd units and  $m$ -period graphene units as  $L_{n,m}$  [see Fig. 1(c)]; this design can be characterized by a pair of integers  $n$  and  $m$ .

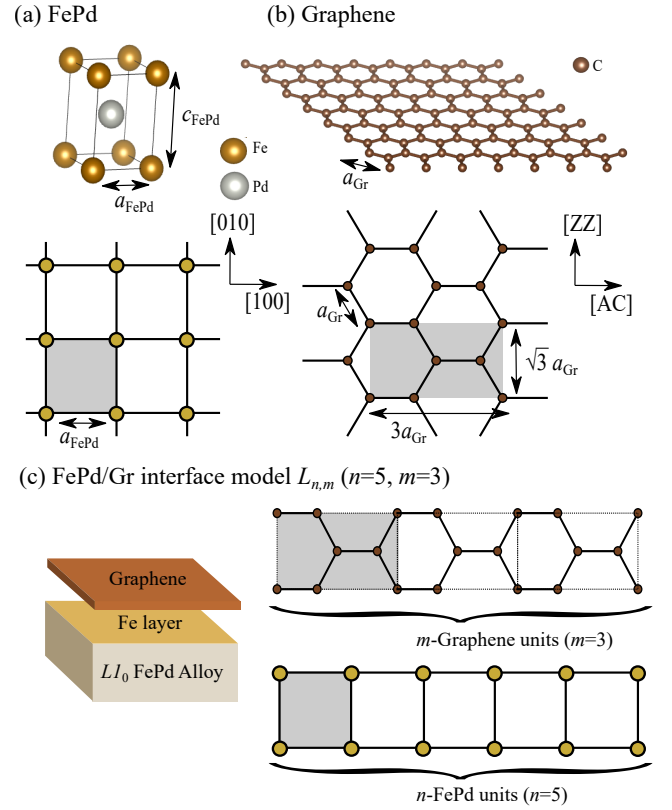


FIG. 1. Conceptual illustration of considered model. (a) Bulk  $L1_0$ -FePd crystal structure and square Fe lattice on the (001) plane. (b) Bulk-graphene structure. The periodic units of the both structures are marked as gray colored areas. (c)  $L_{nm}$  interface structure consisting of  $n$ -FePd units and  $m$ -graphene periodic units ( $n = 5, m = 3$ ).

To understand the atomic-scale structure and electronic properties of the FePd(001)/Gr interface, we performed density functional theory (DFT) calculations using the Vienna ab initio simulation package (VASP) 6.2 code, which uses the projector augmented wave (PAW) method<sup>19</sup> and a plane-wave basis set. We also employed the generalized gradient approximation (GGA) exchange-correlation functional of Perdew–Burke–Ernzerhof (PBE)<sup>20</sup> with Grimme’s DFT-D2 method for vdW interactions<sup>21</sup>.

To evaluate the stability of the  $L_{n,m}$  interface structure, we consider slab supercells, as shown in Fig. 2, which consist of seven atomic layers of FePd with a graphene layer terminating the top side of the slab. The bottom two layers are fixed to simulate bulk properties during the structural optimization. We also used a vacuum layer of approximately  $8.0 \text{ \AA}$ , which is sufficiently large to truncate the interactions by periodic boundary conditions. The initial interlayer distance between the top Fe layer and graphene ( $d_{\text{FeC}}$ ) was determined to be  $2.0 \text{ \AA}$ . Then, the diameter of the  $L_{n,m}$  supercell is  $2.67n \text{ \AA} \times 2.67 \text{ \AA} \times 21.1 \text{ \AA}$ , and the number of Fe, Pd, and C atoms is  $4n$ ,  $3n$ , and  $4m$  C, respectively. To com-

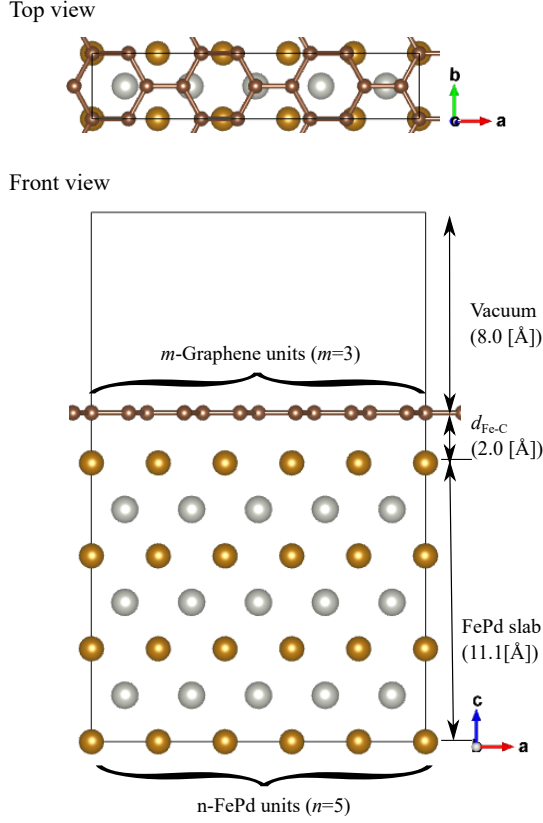


FIG. 2. Computational model of  $L_{nm}$ -type graphene on FePd interface. There are seven atomic layers of FePd, a single carbon layer, and a 8.0 Å vacuum region. The Fe-C interlayer distance was assumed to be 2 Å in the initial condition.

pute such a supercell, the first Brillouin zone was sampled with a  $3 \times 9 \times 1$  Monkhorst-Pack k-point grid; we used a plane wave basis cut-off energy of 400 eV.

### III. RESULT AND DISCUSSION

Here, we consider seven different  $L_{n,m}$ -type interface structures ( $L_{3,2}$ ,  $L_{4,2}$ ,  $L_{4,3}$ ,  $L_{5,3}$ ,  $L_{5,4}$ ,  $L_{7,4}$ , and  $L_{7,5}$ ). To determine their stability, we introduce the binding energy  $E_B(n,m)$  calculated using the following formula:

$$E_B(n,m) = \frac{E_{\text{FePd/Gr}}(n,m) - E_{\text{FePd}}(n) - E_{\text{Gr}}(m)}{N_C(m)} \quad (1)$$

with the number of C atoms  $N_C(m) = 4m$ , where  $E_{\text{FePd/Gr}}(n,m)$  is the total energy of the FePd(001)/Gr slab structure and  $E_{\text{FePd}}(n)$  is that of the pristine FePd slab.  $E_{\text{Gr}}(m)$  is the total energy of the pristine graphene without strain.

Table I shows the binding energies of the seven considered  $L$ -type structures. Most of the structures have a positive  $E_B$  value which is energetically unstable; only two structures indicate negative  $E_B$ .  $L_{5,3}$  is the most

TABLE I. The binding energies  $E_B$  of the  $L_{n,m}$  structures, the total energy of the supercell  $E_{\text{FePd/Gr}}$  and  $n/m$  ratio are also shown in the table.

Model $L_{n,m}$	$n/m$	$E_{\text{FePd/Gr}}$ (eV)	$E_B$ (eV)
$L_{3,2}$	1.50	-223.146	-0.020
$L_{4,2}$	2.00	-270.669	+0.241
$L_{4,3}$	1.33	-306.549	+0.267
$L_{5,3}$	1.67	-360.669	-0.109
$L_{5,4}$	1.25	-390.565	+0.297
$L_{7,4}$	1.75	-495.582	+0.005
$L_{7,5}$	1.40	-530.296	+0.127

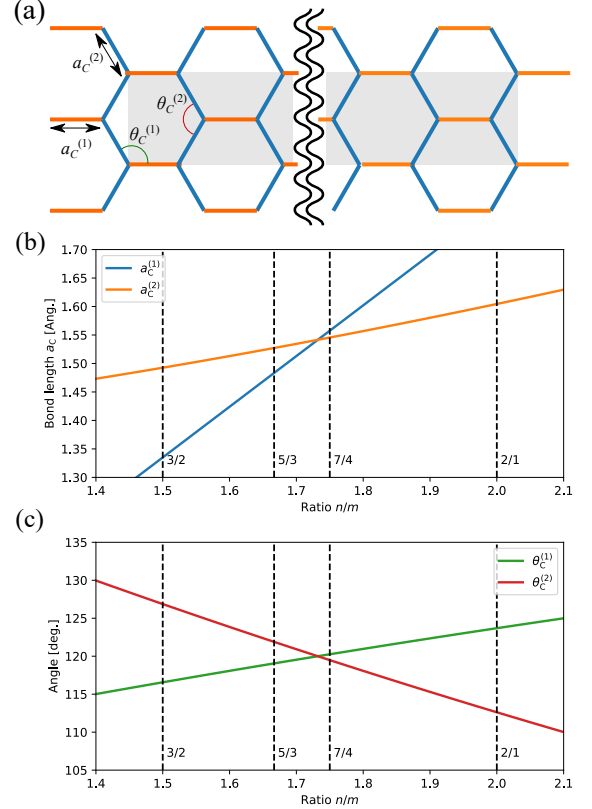


FIG. 3. Estimated modulation of the bond length and bond angle of the carbon layer in the  $L_{nm}$  structure. (a) Definition of bond length  $a_C^{(1)}$ ,  $a_C^{(2)}$ , and bond angle  $\theta_C^{(1)}$ ,  $\theta_C^{(2)}$ . (b)  $a_C^{(1)}$  and  $a_C^{(2)}$  as functions of the  $n/m$  ratio. (c)  $\theta_C^{(1)}$  and  $\theta_C^{(2)}$  as functions of the  $n/m$  ratio.

stable with  $E_B = -0.109$  eV/atom. the next most stable structure is  $L_{3,2}$ . A stable structure always has  $n/m$  between 1.5 ~ 1.7. We suppose that this trend originates from the distortion of the honeycomb structure of graphene.

Then, we consider the bond length and bond angle distributions in the initial state of the optimization. The initial coordinates of the C atoms were obtained by transforming the original graphene into a super cell of size  $na_{\text{FePd}} \times a_{\text{FePd}}$ . After the transformation, the bond lengths are represented by two lengths  $a_C^{(1)}$  and  $a_C^{(2)}$ , as

shown in Fig. 3(a);  $a_C^{(1)}$  and  $a_C^{(2)}$  can be analytically expressed as a function of the ratio,  $n/m$ :

$$a_C^{(1)} = \frac{1}{3} \left( \frac{n}{m} \right) a_{\text{FePd}} \quad (2)$$

$$a_C^{(2)} = \sqrt{\frac{1}{4} + \frac{1}{36} \left( \frac{n}{m} \right)^2} a_{\text{FePd}}. \quad (3)$$

In Fig. 3(b), we plot the  $n/m$  dependence of  $a_C^{(1)}$  and  $a_C^{(2)}$ . Since the equilibrium bond length of the graphene is approximately  $a_{\text{Gr}} = 1.42$  Å, to reduce the strain, the value of  $n/m$  should be approximately  $\approx 1.5$ . Using a similar procedure, the bond angles  $\theta_C^{(1)}$  and  $\theta_C^{(2)}$  in Fig. 3(a) can be calculated using the following equation:

$$\theta_C^{(1)} = \cos^{-1} \left[ -\frac{(n/m)}{6\sqrt{1/4 + (1/36)(n/m)^2}} \right] \quad (4)$$

$$\theta_C^{(2)} = 2 \cos^{-1} \left[ \frac{(n/m)}{6\sqrt{1/4 + (1/36)(n/m)^2}} \right]. \quad (5)$$

Figure 3(c) shows the  $n/m$  dependence of  $\theta_C^{(1)}$  and  $\theta_C^{(2)}$ ; the angle approaches  $120^\circ$  around  $n/m \approx 1.7$ . This result predicts that the distortion of the graphene lattice is minimized in the  $n/m$  range of  $1.5 \sim 1.7$ , which is consistent with Table I).

For the most stable  $L_{5,3}$  structure, the mismatch in the bond angle is less than  $2^\circ$ . On the other hand, the mismatch of the lattice constant  $a_{\text{Gr}}$  reaches  $\sim 7.5$  %, which is much higher than 1.3 % in Ni(111)/Gr<sup>22</sup>. Despite the large strain energy, the binding energy of  $L_{5,3}$  was  $-0.109$  eV/atom ( $\sim -10.5$  kJ/mol), which is comparable to the  $-12$  kJ/mol of Ni(111)/Gr<sup>14</sup>. Thus, we believe this structure is thermodynamically stable.

We also consider the twisted interface models as shown in Fig. 4. Because low-strain structures are energetically stable, as shown in the above results, we explored the initial structures in the range of  $a_C < 1.6$  Å and  $115^\circ < \theta_C < 125^\circ$  and obtain three available supercells consisting of less than 25 carbon atoms, which are labeled as  $T_{n,m+1/2}$  in Fig. 4(a)-(c). In Table II, we present the geometrical parameters and binding energies.  $\theta$  represents the twist angle between the FePd (100) axis and the AC axis of graphene. We also calculated the mean absolute error (MAE) of the bond angle of the carbon atoms from  $120^\circ$  and the MAE of the bond length  $a_C/a_{\text{Gr}}$ . Figure 4(c) has relatively low distortion and is as stable as the linear  $L_{5,3}$  structure.

Next, we calculated the potential energy surface (PES) profile: adsorption-energy dependency on the lateral displacement of a single C atom with respect to the top-most Fe atom. Figure 5(a) shows the schematic illustration;  $\Delta x$  and  $\Delta y$  represent the magnitudes of the displacements. Structural optimizations were performed by fixing the lateral position of the  $C_1$  atom and obtaining the binding energy as a function of the displacement  $E_B(n, m; \Delta x, \Delta y)$ . Figure 5(b) plots  $\Delta E(\Delta x, \Delta y)$  de-

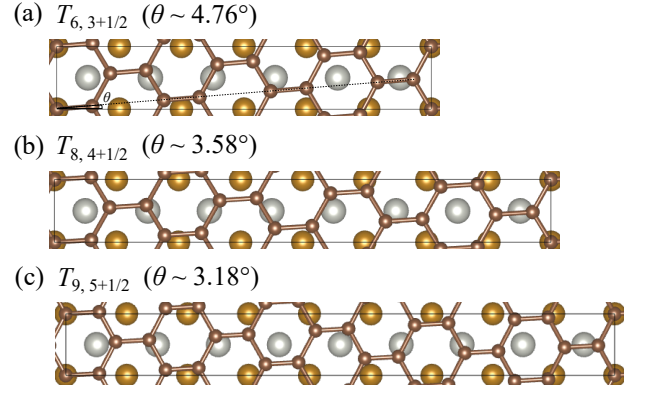


FIG. 4. Twisted FePd(001)/Gr interface models with different twist angles.

TABLE II. The geometrical parameters and binding energies of the twisted interface structure shown in Fig. 4(a)-(c). The twist angle  $\theta$  and the mean absolute error (MAE) of the bonding angle  $\theta_C$  and length  $a_C$  from the graphene in the equilibrium condition were also calculated.

Name	$\theta$	MAE $\theta_C$	MAE $a_C/a_{\text{Gr}}$	$E_B$ (eV/atom)
(a) $T_{6,3+1/2}$	$4.76^\circ$	$2.53^\circ$	8.1 %	0.005
(b) $T_{8,4+1/2}$	$3.58^\circ$	$2.21^\circ$	10 %	0.097
(c) $T_{9,5+1/2}$	$3.18^\circ$	$2.55^\circ$	5.6 %	-0.095

fined as:

$$\Delta E(\Delta x, \Delta y) = E_B(n, m; \Delta x, \Delta y) - E_B(n, m; 0, 0). \quad (6)$$

Because of the translational symmetry of the system, the equivalent points appear periodically in the PES profile. The energetically stable minimum appears in the vicinity of  $(\Delta x, \Delta y) = (0, 0)$ , which corresponds to the case when a single C atom is at the top of the Fe site, and  $\Delta E$  becomes unstable when every C atom is equally distant from the Fe atoms. This sub- $a_{\text{Fe}}$  scale change is a result of the attractive short-range interaction between Fe and C atoms, which reflects the existence of chemisorption. In contrast, the change in  $\Delta E$  does not exceed 0.006 eV/atom. Because it is less than 5 % of the adsorption energy gain, the adsorption state is considered to be stable against lateral shifts. In addition, this 5 % change is largely below the typical value obtained for chemisorption on fcc metals such as Ni(111)/Gr<sup>14</sup>; it is relatively close to the order of the physisorbed case.

Figure 6 shows the electron density profile of the  $L_{5,3}$  structure. A high-density area is found between labelled  $C_1$  and the neighboring C atom, which represents a C-C  $sp^2\sigma$  bond orbital. Although most C – Fe bonds are not clearly seen as C – C, there is an area of slightly higher density between  $C_1$  and  $Fe_1$  (displayed by the broken circle), which is one of the closest Fe-C pairs. In addition, the average Fe-C binding distance is approximately 2 Å, which is a typical value for chemisorbed metal/Gr interfaces<sup>14,23</sup>. The graphene surface is slightly bumpy on the atomic scale; the vertical position of the  $C_1$  atom

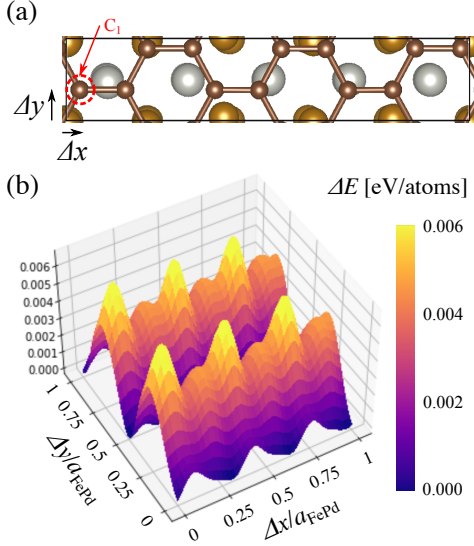


FIG. 5. Potential energy surface for lateral shifts of the graphene layer on FePd(001). (a) Schematic illustration.  $\Delta x$  and  $\Delta y$  represent the displacements of the  $C_1$  atom from the top of a single Fe site. (b) Dependence of the binding energy difference  $\Delta E$  on  $(\Delta x, \Delta y)$ .

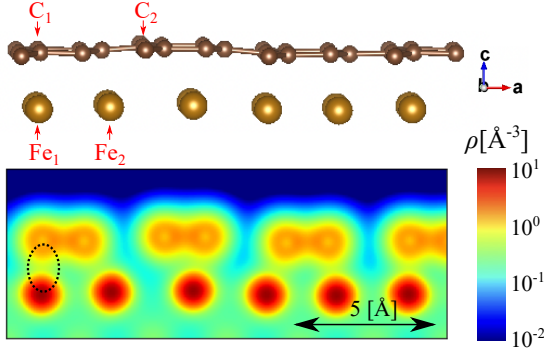


FIG. 6. Charge density profile of the  $L_{5,3}$ -type FePd(001)/Gr interface.  $C_1$  and  $Fe_1$  represent the closest pair, and  $C_2$  and  $Fe_2$  are examples of sites with no close C or Fe atoms.

is approximately 0.0? Å lower than that of the  $C_2$  atom. This seems to be a result of the Fe-C attractive interaction, which is also seen in Fig. 5(b).

Figure 7 shows the density of states (DoS) of the pristine FePd(001) and FePd(001)/Gr slab; the positive and negative curves represent majority and minority spin. In Fig. 7(a)–(b), the total DoS (tDoS) has no significant difference owing to the presence of the graphene layer. The slight change in the tDoS around  $-10 \sim -5$  eV originates at the 2p level of graphene. Figure 7(c)–(d) represent projected DoS (pDoS) on the top layer Fe atoms. The  $d$  orbitals exhibit large exchange splitting around the Fermi level representing ferromagnetic order, which is not significantly degraded by the pres-

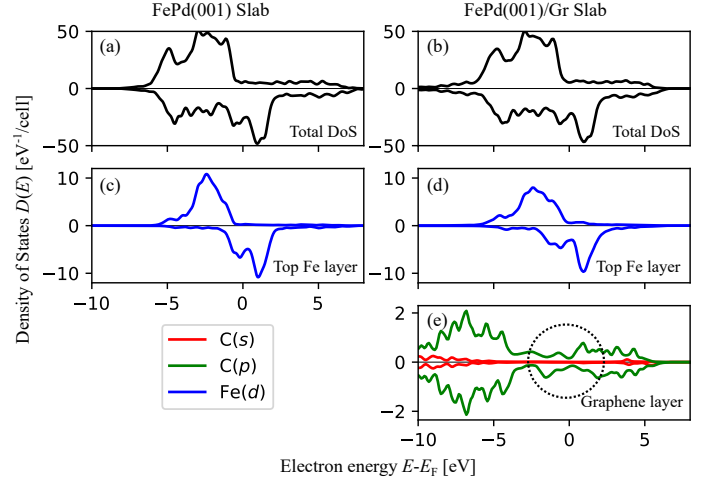


FIG. 7. Density of states (DoS) for the pristine FePd(001) slab (left) and FePd(001)/Gr slab (right) (a)–(b) Total DoS (c)–(d) projected DoS (pDoS) on the top layer Fe atoms. (e) pDoS on the C atoms.

ence of graphene. This behavior is consistent with recent experimental measurements<sup>6</sup>, which indicate that the macroscopic ferromagnetic property is conserved in FePd/Gr. The bottom panel represents the pDoS on the graphene. Although free-standing graphene is originally non-magnetic, there is an asymmetry between the minority and majority spins near the Fermi level, which represents the magnetization of the graphene. The magnitude of the local spin magnetic moment of a carbon atom was less than  $0.02 \mu_B/\text{atom}$ . This is slightly lower than the reported induced magnetic moments on ferromagnetic surfaces ( $\sim 0.05 \mu_B/\text{atom}$  for Ni(111)/Gr)<sup>17</sup>. This is considered to originate from the transfer of electrons due to the interaction between the  $C(p)$  and  $Fe(d)$  orbitals.

Next, we consider the radial distribution function of C-Fe bonds, which is defined as follows:

$$d(r) = \sum_i^{(\text{Fe})} \sum_j^{(\text{C})} \delta(r - r_{ij}), \quad (7)$$

where  $r_{ij}$  represents the distance between the  $i$  and  $j$ -th atoms, and the summations over  $i$  and  $j$  are performed over the topmost Fe and C atoms, respectively. For computational convenience, we use a Gaussian of  $\sigma = 0.1$  Å as the  $\delta$ -function above. In Fig. 8,  $d(r)$  has a broad band from 2 Å to 3 Å. In previous studies of fcc metals, it is known that the typical chemisorbed distances are approximately 2 Å, and 3 Å for the physisorbed surface. In our FePd, the Fe atoms are arranged along a tetragonal lattice. This is very different from the situation in the fcc(111) plane from the surface metal atoms. As shown in the figure, the nearest neighboring atoms have a distance of 2 Å.

Figure 9(a) shows cross-sectional scanning tunnel electron microscopy (STEM) images of a sample in which

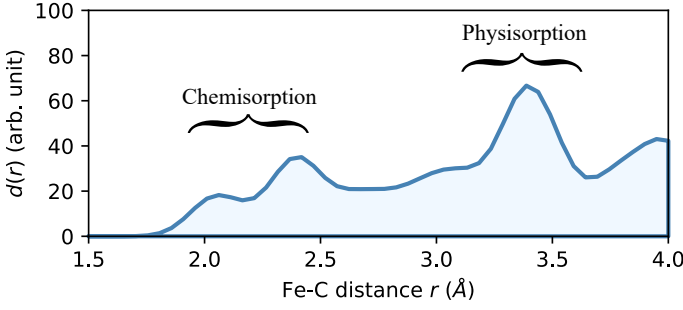


FIG. 8. Radial distribution function of the C-Fe bonds. The typical distances for chemisorption ( $\sim 2$  Å) and physisorption ( $\sim 3$  Å) are labeled for convenience.

three layers of graphene are formed on an epitaxial FePd film. Three complementary detection modes are presented: BF-, ABF, and HAADF. From the BF and ABF-STEM images, it could be confirmed that the interatomic distance between the first layer of graphene and FePd was approximately 1.9 Å, while the upper layers of graphene were approximately 4 Å. The HAADF-STEM image showed that the Fe and Pd were alternatively aligned to the out-of-plane direction, which indicates the highly ordered  $L1_0$  structure. The fact that the top surface layer is Fe agrees with the model shown in Fig. 2. In Fig. 9(b), we show the optimized interatomic distances of single-layer, bilayer, and trilayer graphene on the FePd slab. We assume the ABA stacking order for individual graphene sheets, which provides the lowest formation energy. The distance between graphene and FePd is close to the experimental value. In addition, the distance between the upper layers of graphene tends to increase above 3.5 Å, which is consistent with the experimental results.

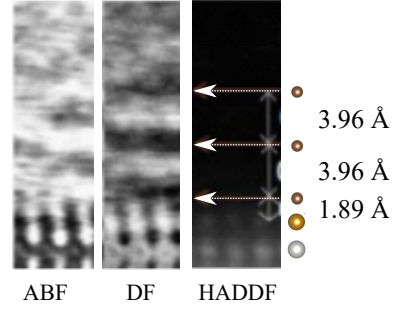
#### IV. SUMMARY

In this work, we studied the interface structures of FePd(001)/Gr using DFT. Simple models for carbon-atom configurations and formulated the conditions to reduce strain of the graphite. From the calculated adsorption energies and their PES profiles, we found that there is a stable adsorption state with  $E_B = -0.109$  eV/atom (10.5 kJ/mol), which is comparable in order of magnitude to that of the well-understood fcc-metal/Gr interface<sup>14</sup>. The calculated interlayer distances well reproduce the experimentally measured values.

Previously, the interface structure and bonding mechanism of fcc-metal(111)/Gr have been studied extensively, and the lattice similarity between the metallic atoms on the (111)-face and C atoms. However, few studies of the tetragonal  $L1_0$ -type surface, which has a significant mismatch in the lattice symmetry, have been reported.

In the FePd(001)/Gr case, the PES profile showed a small change with respect to the atomic scale displacement, but it was relatively flat with respect to the order of the adsorption energy (approximately 5 %). The

(a) Experimental results (Trilayer)



(b) Computational results

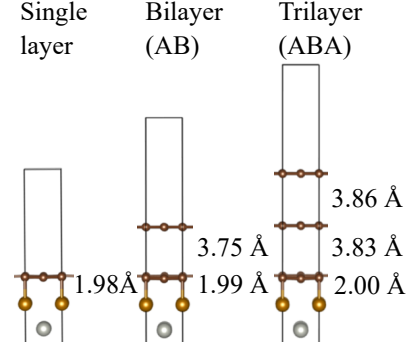


FIG. 9. Comparison of the computational results and observation by the electron microscopy. (a) STEM image of trilayer graphene on FePd interface (a) Estimated inter-Fe-C inter-layer distances of single-layer, bilayer, and trilayer graphene on FePd.

scale of adsorption energy is close to that of chemisorption, but the site selectivity is much smaller than in the case of fcc-metal(111)/Gr, which resembles that of physisorption. The radial distribution function also indicates that the broad peaks reflect both chemisorption and physisorption distances, which coexist owing to the lattice symmetry mismatch. It is natural to assume that the averaging of these two bonding mechanisms is the origin of the intermediate behavior. The weakly hybridized state indicates that the macroscopic electronic and magnetic properties of FePd are not significantly changed by the presence of graphene, which is also in good agreement with the experimental results<sup>6</sup>. We expect that FePd(001)/Gr has desirable properties for MTJ applications. Because the graphene coverage is sufficiently stable to protect the Fe from oxidation without significantly degrading the macroscopic magnetic properties, the FePd/Gr interface can avoid large lattice mismatches such as that exhibited by the FePd/MgO interface.

In addition, we believe that this study provides a starting point for the analysis of the tetragonal alloy/graphene interface, including the lattice symmetry mismatch and their application in electronics and spintronics devices.

## ACKNOWLEDGMENTS

This work was supported by MEXT as "Program for Promoting Researches on the Supercomputer Fugaku" (Quantum-Theory-Based Multiscale Simulations Toward the development of next-generation energy-saving semiconductor devices, JPMXP1020200205) and used the computational resources of super computer Fugaku provided by the RIKEN Center for Computational Science (Project ID: hp200122/hp150273). T.O. acknowledge the financial support from JSPS KAKENHI (grant number:JP16H03865). M.U., H.N., and T.O. acknowledges the JSPS Core-to-Core Program (grant number:JPJSCCA20160005). This work was performed with the approval of the Photon Factory Program Advisory Committee (H.N. and K.A.) (No. 2019S2-003). The visualization of the atomic structures in this study was performed using VESTA software<sup>24</sup>. The computation was performed by the facilities of the Supercomputer Center, the Institute for Solid State Physics, the University of Tokyo, and also performed by Oakforest-PACS at JCAHPC through the Multidisciplinary Cooperative Research Program in CCS, the University of Tsukuba.

## AUTHOR DECLARATIONS

### Conflict of Interest

The authors have no conflicts to disclose.

## DATA AVAILABILITY

The data that support the findings of this study are available from the corresponding author upon reasonable request.

- <sup>1</sup>H. Naganuma, G. Kim, Y. Kawada, N. Inami, K. Hatakeyama, S. Iihama, K. M. Nazrul Islam, M. Oogane, S. Mizukami, and Y. Ando, "Electrical detection of millimeter-waves by magnetic tunnel junctions using perpendicular magnetized  $L1_0$ -FePd free layer," *Nano Lett.* **15**, 623–628 (2015).
- <sup>2</sup>D.-L. Zhang, K. B. Schliep, R. J. Wu, P. Quarterman, D. Reifsnnyder Hickey, Y. Lv, X. Chao, H. Li, J.-Y. Chen, Z. Zhao, *et al.*, "Enhancement of tunneling magnetoresistance by inserting a diffusion barrier in  $L1_0$ -FePd perpendicular magnetic tunnel junctions," *Appl. Phys. Lett.* **112**, 152401 (2018).
- <sup>3</sup>T. Klemmer, D. Hoydick, H. Okumura, B. Zhang, and W. Soffa, "Magnetic hardening and coercivity mechanisms in  $L1_0$  ordered FePd ferromagnets," *Scr. Mater.* **33**, 1793–1805 (1995).
- <sup>4</sup>H. Shima, K. Oikawa, A. Fujita, K. Fukamichi, K. Ishida, and A. Sakuma, "Lattice axial ratio and large uniaxial magnetocrystalline anisotropy in  $L1_0$ -type FePd single crystals prepared under compressive stress," *Phys. Rev. B* **70**, 224408 (2004).
- <sup>5</sup>N. Miyata, H. Asami, T. Mizushima, and K. Sato, "Ferromagnetic Crystalline Anisotropy of  $Pd_{1-x}Fe_x$  Alloys. III. 0.38  $\sim$  0.5,

- $L1_0$ -Type Ordered Phase," *J. Phys. Soc. Jpn.* **59**, 1817–1824 (1990).
- <sup>6</sup>H. Naganuma, V. Zlatko, M. Galbiati, F. Godel, A. Sander, C. Carr  tero, O. Bezencenet, N. Reyren, M.-B. Martin, B. Dlubak, *et al.*, "A perpendicular graphene/ferromagnet electrode for spintronics," *Appl. Phys. Lett.* **116**, 173101 (2020).
- <sup>7</sup>T. Mohri, T. Horiuchi, H. Uzawa, M. Ibaragi, M. Igarashi, and F. Abe, "Theoretical investigation of  $L1_0$ -disorder phase equilibria in Fe-Pd alloy system," *J. Alloys Compd.* **317**, 13–18 (2001).
- <sup>8</sup>S. Iihama, A. Sakuma, H. Naganuma, M. Oogane, T. Miyazaki, S. Mizukami, and Y. Ando, "Low precessional damping observed for  $L1_0$ -ordered FePd epitaxial thin films with large perpendicular magnetic anisotropy," *Appl. Phys. Lett.* **105**, 142403 (2014).
- <sup>9</sup>T. Kawai, A. Itabashi, M. Ohtake, S. Takeda, and M. Futamoto, "Gilbert damping constant of FePd alloy thin films estimated by broadband ferromagnetic resonance," in *EPJ Web of Conferences*, Vol. 75 (EDP Sciences, 2014) p. 02002.
- <sup>10</sup>S. Zharkov, E. Moiseenko, R. Altunin, N. Nikolaeva, V. Zhihalov, and V. Myagkov, "Study of solid-state reactions and order-disorder transitions in Pd/ $\alpha$ -Fe (001) thin films," *JETP Lett.* **99**, 405–409 (2014).
- <sup>11</sup>A. Itabashi, M. Ohtake, S. Ouchi, F. Kirino, and M. Futamoto, "Preparation of  $L1_0$  ordered FePd, FePt, and CoPt thin films with flat surfaces on MgO (001) single-crystal substrates," in *EPJ Web of Conferences*, Vol. 40 (EDP Sciences, 2013) p. 07001.
- <sup>12</sup>A. D. Kent and D. C. Worledge, "A new spin on magnetic memories," *Nat. Nanotechnol.* **10**, 187–191 (2015).
- <sup>13</sup>G. Bertoni, L. Calmels, A. Altibelli, and V. Serin, "First-principles calculation of the electronic structure and EELS spectra at the graphene/Ni (111) interface," *Phys. Rev. B* **71**, 075402 (2005).
- <sup>14</sup>S. M. Kozlov, F. Vines, and A. G  rling, "Bonding Mechanisms of Graphene on Metal Surfaces," *J. Phys. Chem. C* **116**, 7360–7366 (2012).
- <sup>15</sup>I. Hamada and M. Otani, "Comparative van der Waals density-functional study of graphene on metal surfaces," *Phys. Rev. B* **82**, 153412 (2010).
- <sup>16</sup>A. Varykhalov, J. S  nchez-Barriga, A. M. Shikin, C. Biswas, E. Vescovo, A. Rybkin, D. Marchenko, and O. Rader, "Electronic and Magnetic Properties of Quasifreestanding Graphene on Ni," *Phys. Rev. Lett.* **101**, 157601 (2008).
- <sup>17</sup>T. Abtew, B.-C. Shih, S. Banerjee, and P. Zhang, "Graphene-ferromagnet interfaces: hybridization, magnetization and charge transfer," *Nanoscale* **5**, 1902–1909 (2013).
- <sup>18</sup>F. Mittendorfer, A. Garhofer, J. Redinger, J. Klimes  , J. Harl, and G. Kresse, "Graphene on ni(111): Strong interaction and weak adsorption," *Phys. Rev. B* **84**, 201401 (2011).
- <sup>19</sup>P. E. Bl  chl, "Projector augmented-wave method," *Phys. Rev. B* **50**, 17953 (1994).
- <sup>20</sup>J. P. Perdew, K. Burke, and M. Ernzerhof, "Generalized gradient approximation made simple," *Phys. Rev. Lett.* **77**, 3865 (1996).
- <sup>21</sup>S. Grimme, "Semiempirical GGA-type density functional constructed with a long-range dispersion correction," *J. Comp. Chem.* **27**, 1787–1799 (2006).
- <sup>22</sup>M. Hasegawa, K. Nishidate, T. Hosokai, and N. Yoshimoto, "Electronic-structure modification of graphene on ni (111) surface by the intercalation of a noble metal," *Phys. Rev. B* **87**, 085439 (2013).
- <sup>23</sup>M. Piquem  l-Banci, R. Galceran, S. M.-M. Dubois, V. Zlatko, M. Galbiati, F. Godel, M.-B. Martin, R. S. Weatherup, F. Petroff, A. Fert, *et al.*, "Spin filtering by proximity effects at hybridized interfaces in spin-valves with 2D graphene barriers," *Nat. Commun.* **11**, 1–9 (2020).
- <sup>24</sup>K. Momma and F. Izumi, "VESTA 3 for three-dimensional visualization of crystal, volumetric and morphology data," *J. Appl. Crystallogr.* **44**, 1272–1276 (2011).